Available online at www.sciencedirect.com
ScienceDirect
Journal of Power Sources 162 (2006) 620–628
JOURNAL OF POWER SOURCES
www.elsevier.com/locate/jpowsour

Carbon nanotube/felt composite electrodes without polymer binders

J. Mauricio Rosolen *, E.Y. Matsubara, Marcel S. Marchesin, Stella M. Lala, L.A. Montoro, S. Tronto

Departamento de Química-FFCLRP, Universidade de São Paulo, Ribeirão Preto 14040-930, SP, Brazil

Received 2 June 2006; received in revised form 28 June 2006; accepted 28 June 2006
Available online 14 August 2006

Abstract

In this work we have investigated the suitability of composite electrodes consisting of cup-stacked and bamboo-like carbon nanotubes (CNT) synthesized directly onto a carbon felt for both lithium storage and double-layer capacitance applications. The CNT/felt composite electrode was prepared using catalytic chemical vapor decomposition on the carbon felt. The microstructure of the electrodes was characterized by scanning electron microscopy. Electrochemical characterization of the CNT/felt, either submitted or not to acid treatment for extraction of the catalytic particles used during the CNT growth, was carried out using 1 mol L^{-1} $LiPF_6$ in mixtures of ethylene carbonate, dimethyl carbonate, diethyl carbonate, and propylene carbonate. The carbon nanotubes loading and the type of CNT, whether open or closed, on the felt were the most significant factors regarding the electrochemical properties of the composite. With respect to the application of the composite to lithium storage, an anomalous behavior in the reversible specific capacity as a function of the current was detected. The capacity was found to be large at higher current values. The best reversible specific capacity was found for the open-CNT/felt (275 mAh g^{-1} at 0.16 A g^{-1}, and 200 mAh g^{-1} at 0.82 A g^{-1}), on an area of 0.634 mm^2. The double-layer capacitance of the CNT decreased with increasing current. In the case of the open-CNT with a CNT loading of 13.93 mg, the composite provided 40.3 μF cm^2 or about 12 F g^{-1} at 10 mA of polarization current using 1 mol L^{-1} $LiPF_6$ in mixtures of ethylene carbonate and dimethyl carbonate. For the closed-CNT with a CNT loading of 9.3 mg, the double-layer capacitance was 30 F g^{-1} at 20 mA in 1 M H_2SO_4.

Keywords: Carbon nanotubes; Carbon composite; Capacitor; Li-ion battery; Cup-stacked carbon

1. Introduction

It is well-known that most of the electrodes used in the preparation of Li-ion batteries and capacitors contain some kind of polymeric binder [1,2]. The binder (e.g. teflon, polyvinylidene fluoride) is often used to allow the preparation of pellets or membrane electrodes, since it aggregates the active and additional materials comprising the electrode. In spite of this role, it also appears as a drawback for the development of these devices. For instance, the presence of a binder in the electrode reduces the effective area of active material that is exposed to the electrolyte, as well as the percolation of the latter. It also often limits the temperature range over which the device can work because of its thermal stability, which is frequently lower than the thermal stability of the active materials such as carbon or oxides commonly used in capacitors, lithium battery and fuel cells. The electrical resistance of the electrode containing a binder is also higher than that of a binder-free electrode.

In this work, we have investigated binder-free composite electrodes based on cup-stacked and bamboo-like carbon nanotubes and carbon felt. Carbon nanotubes are new materials for the development and potential improvement of fuel cells, lithium ion batteries, and capacitors because of their unique electrical and chemical properties [3,4]. Carbon nanotubes appear to be electronically conductive supports or substrates for catalytic nanoparticles, polymers, oxides, proteins, and many other classes of materials. Cup-stacked and bamboo-like carbon nanotubes are structures that have been less frequently studied for electrochemical applications when compared with MWCNT and SWCNTs. Cup-stacked carbon nanotubes have been proposed as a good alternative for the direct methanol fuel cell, while carbon nanotubes with a bamboo-like structure have been studied for the lithium electrode [5–7].

* Corresponding author. Tel.: +55 16 3602 3787; fax: +55 16 3602 4838.
E-mail address: rosolen@ffclrp.usp.br (J.M. Rosolen).

0378-7753/$ – see front matter © 2006 Elsevier B.V. All rights reserved.
doi:10.1016/j.jpowsour.2006.06.087

The CNT/felt electrode can be defined as a three-dimensional web of electronic conductive carbon fiber with excellent mechanical properties, which can be submitted to several chemical treatments such as those used for functionalization, purification, and aggregation of nanoparticles on CNTs. In addition, the CNT/felt is a lightweight electrode with both the thermal stability of felt and CNTs. It also has a low impedance because the felt material is an excellent electron conductor.

2. Experimental details

The CNT/felt electrode was obtained by growing CNT via decomposition of methanol on cobalt and manganese metallic particles deposited on a carbon felt, as described in detail in reference [8]. This was accomplished by means of a fixed-bed flow reactor at a temperature of 650 °C, under nitrogen flow, to carry the methanol solvent vapor away. A low area carbon felt was produced from a polyacrylonitrile (PAN) precursor and its electronic conductivity was about 0.96 $\Omega\,cm^{-1}$ [9].

Before the CNT growth was performed, the felts were cut in to the shape of a disc with a diameter of 7 mm and a thickness of about 1 mm. The felt mass was determined before catalyst incorporation, and the final mass of the CNT/felt electrode was also measured. The latter electrode consisted of growing CNT mass together with the catalytic particles used in the CNT growth. The CNT mass in the composite was determined using thermogravimetric analyses in N_2. Felts containing the catalytic mixture were heated to 650 °C in N_2, and the mass change was determined. In this work, the total capacity or total capacitance was obtained using the mass of the felt, CNT, and catalyst (i.e., the total mass of the electrode), while the specific capacity and specific capacitance were calculated using the CNT mass in the CNT/felt composite.

Some electrodes were also submitted to reflux with concentrated HCl under magnetic stirring for 6 h at 50 °C, and then dried under vacuum at 100 °C. This procedure was applied to remove the catalytic particles in the CNT/felt as detected by electron dispersive spectroscopy.

Electrochemical characterization was performed in a button cell (8 mm diameter) at room temperature. Metallic lithium was used as the auxiliary and reference electrodes. The electrolyte was a 1 mol L^{-1} solution of $LiPF_6$ in dimethyl carbonate, DMC; diethyl carbonate, DEC; propylene carbonate, PC (Selectipur-3:1:1, w/w) or dimethyl carbonate; DMC and ethylene carbonate-EC (Selectipur-1:1, w/w). The separators consisted of polypropylene membrane (Celgard-2400). The voltammograms were obtained by using a PAR-364 potentiostat/galvanostat, while the discharge/charge cycles were controlled by a potentiostat/galvanostat, MacPile or PAR-Labview (capacitance measurements). The electrodes were submitted to vacuum at 100 °C before assembly of the cells in a dry-box (MBraum).

Nitrogen adsorption measurements at 77 K were carried out using a Quantachrome NOVA 1200 equipment, after pre-evacuation for 3 h at 150 °C. Scanning electron microscopy was conducted on a JEOL, JSM 6330F instrument (SEM, field emission gun) operating at 25 kV.

3. Results and discussion

Fig. 1a shows the optical image of a typical CNT/felt electrode, while Fig. 1b shows SEM images of a typical fiber of a CNT/felt electrode. In the optical image, it is possible to see that the CNT/felt is a three-dimensional web electrode. Sectional cuts of the electrode reveal that CNTs can be found all over the electrodes since chemical impregnation was used to disperse the Mn, Co catalysts. Fig. 1b shows that the surface of each single fiber exhibited a uniform CNT coating. The deposit was cotton-like, and covered all the regions of the exposed felt, thus resembling an outer coating or collar on each fiber. However, the CNT/felts observed by SEM pictures reveal that the quality of the CNT deposit depends on both catalyst (Mn, Co) loading and the reaction parameters such as the methanol flux and the reaction time. In the case of the CNT/felt composites studied in this work, we verified that the samples with a lower CNT mass generally had carbon fibers that did not contain carbon nanotubes, as shown in Fig. 1. For example, for a CNT loading lower than 2 mg, the fiber of the felt contained a CNT deposit that resembled thorns. Thus, the CNT mass mounted on the composite or the CNT loading on the composite is a parameter that can be correlated indirectly with several properties of the CNT/felt. In fact, in our previous study concerning the electron field emission of carbon nanotubes on a carbon felt, the CNT loading was a determining factor for the electronic properties of the CNT/felt, as probed by emission. In this study [10], we concluded that the mass reflected the number of carbon nanotubes on the felt as well as the electronic interactions between them. This means that the CNT loading on the composite must reflect the number of sites for lithium intercalation and/or adsorption of chemical species. In addition, the CNT loading should affect the potential of these sites with respect to the intercalation or adsorption of chemical species, since the electronic properties of one tube was different from those of several connected tubes. The CNT loading also affected the mechanical properties of the composite. The CNT/felt with a lower CNT loading was more flexible and coiled to be easily bent, while the CNT/felt with a higher loading became rigid. These differences occured because the big cavities that comprised the structure of the felt were filled with the CNTs (see Fig. 1). Thus, it is reasonable to suppose that these spaces in the felt structure are occupied by CNT which should affect the electrical resistance of the composite electrode too. In a study on the CNT/diamond/felt emission, it was verified that the electronic conductivity of the fiber decreased upon CNT growth [8].

Transmission electron microscopy (TEM) pictures, not presented here, showed that a large majority of the CNTs grown on the felt had an average tube diameter of about 15 nm. In previous work on electron emission of CNT/felt prepared under the same conditions we found that the CNTs covering the fiber of the felt consisted mainly of nanostructures of the cup-stacked and bamboo-like types. Fig. 1c shows an electronic transmission picture of the cup-stacked CNT found in the CNT/felt, a fiber with a stacking morphology of truncated conical graphene, large amounts of open edges on the outer surface and empty central channels. For the bamboo-like structure, the stacking may not

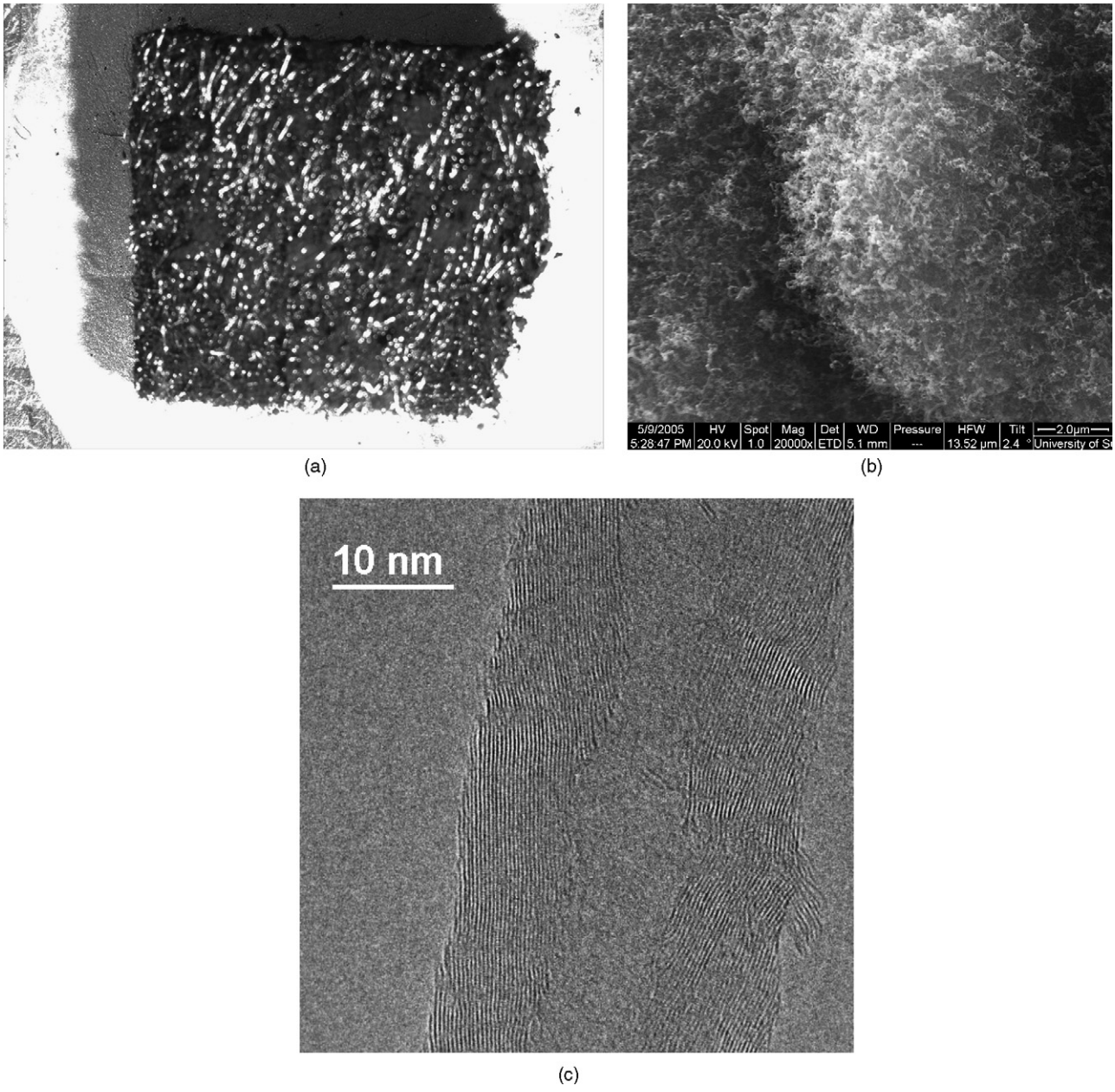

Fig. 1. Picture of a typical CNT/felt electrode (a), SEM picture of the CNT/felt showing the fibers of the CNT/felt electrode in detail (b), and a high resolution transmission electronic microscopy of the carbon nanotube predominantly found in the CNT/felt electrodes (c).

be organized as in the case of the cup-stacked CNTs, and the tubes have nodes in the central channels, while the channel of the cup-stacked CNT is hollow. TEM pictures not shown here revealed that the HCl treatment extracted the catalyst from the tips of the tubes, leaving them open. Thus, we have two kinds of compounds: the closed-CNTs/felt and the open-CNTs/felt or composite that contains CNTs with open tubes.

The specific surface area (SSA) of the CNT/felt was measured using the BET method and it was found that it was controlled by the carbon nanotubes. To obtain an accurate measure of the SSA of the CNT/felt, it was necessary to use several electrodes with different CNT loadings. For a closed-CNT loading of 37.8 mg the SSA is about 148 $m^2\ g^{-1}$, while the SSA is about 109 $m^2\ g^{-1}$ to 17.3 mg of open-CNTs. In the case of felt the SSA is only 1.0 $m^2\ g^{-1}$. From N_2 adsorption isotherm data it was also possible see that the felt and the CNT/felt are non-porous composites.

The electrochemical responses of the CNT/felt and the felt alone at a very low potential scan (0.1 $mV\ s^{-1}$) are shown in Fig. 2. Fig. 2a shows the voltammogram of the felt, while that of the closed-CNT/felt is shown in Fig. 2b–d, and the voltammogram of open-CNT/felt is in Fig. 2c.

All the voltammograms in Fig. 2 display an imbalance between the cathodic and anodic charges that vanish or decrease in the second cycle. They also have cathodic peaks in the first scan that disappear or are drastically modified in successive cyclic potential sweeps. The felt voltammogram (Fig. 2a) displays only one anodic process, and it shows that there is no anodic electrolyte decomposition, thus confirming the quality of

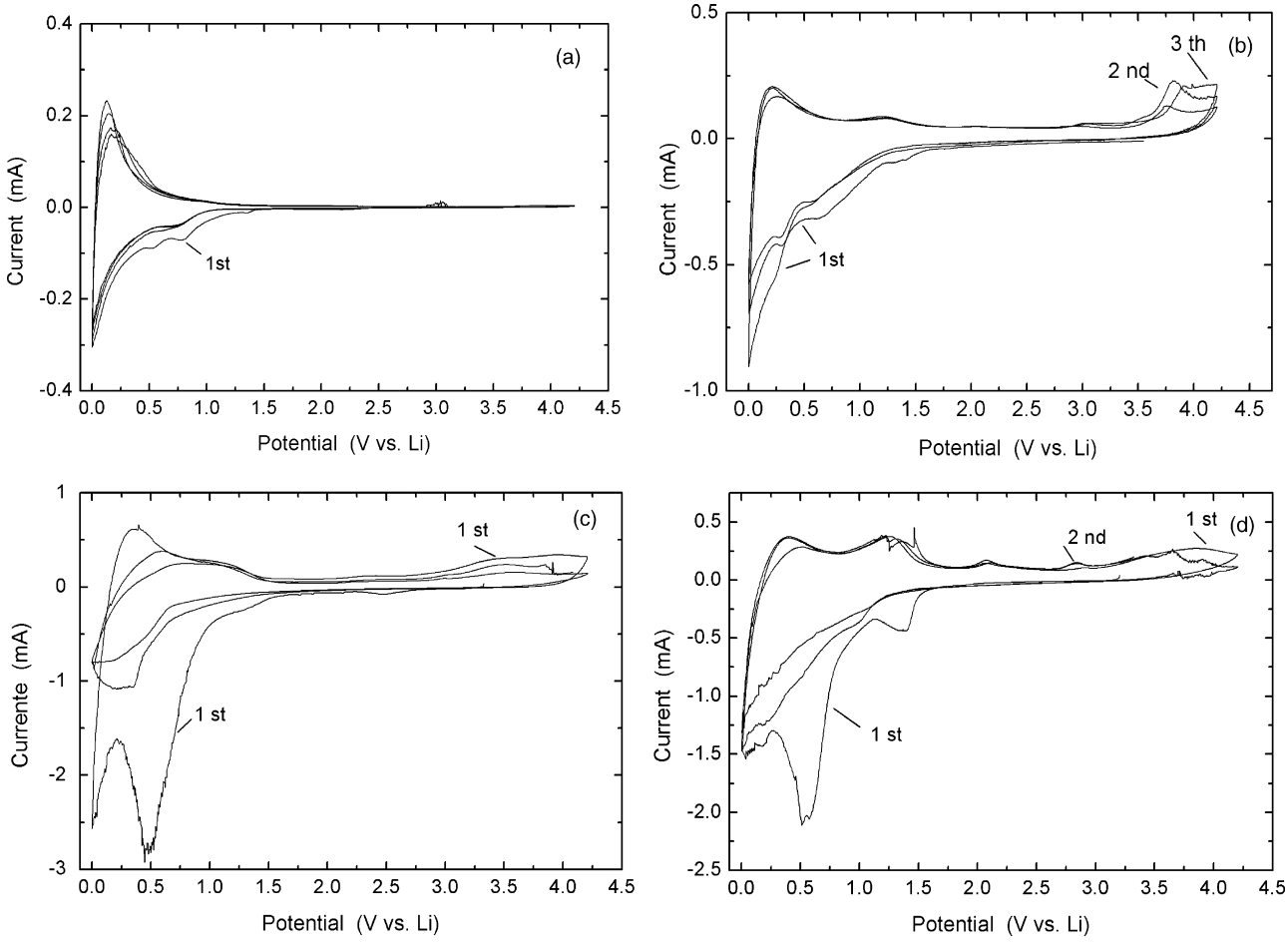

Fig. 2. Voltammograms collected at low scan rate (0.1 mV s^{-1}) for the felt (a), the closed-CNT/felt (b), the open-CNT/felt (c) in EC/DMC, and for the closed-CNT/felt in PC/DEC/DMC (d). The CNT mass growth on the felt is 1.07 mg in (b), 9.43 mg in (c), and 11.3 mg in (d).

the electrolyte used in this study. The CNT/felt contains several anodic peaks and a capacitive current appears after the second anodic peak. In addition, other anodic peaks are observed for the CNT/felts over 1.5 V.

The behavior in the voltammograms shown in Fig. 2 can be partially rationalized if one takes into account the hundreds of studies on lithium intercalation in carbonaceous electrodes and nanotubes [1,11–14]. Lithium insertion in open-CNTs could also occur inside the tube channels, in the wall of defective MWCNTs, in the layer of CNTs, and eventually in micropores resulting from the agglomeration of SWCNTs, and MWCNTs ropes or beams. Li/Li^+ is also preferably located near the carbon nanotube side walls, instead of being in the center of the tube. Some of these sites can allow the co-intercalation of solvent molecules too.

In the case of our CNT/felt, the nanotubes were grown by using chemical vapor decomposition. In this method, it is well known that the tubes are fixed perpendicularly to the surface of the substrate in a way that the pore size distribution is expected to be lower than in the case of randomly agglomerated tubes (for example, powder samples), as confirmed by the N_2 adsorption isotherm analyses. This means that lithium intercalation into the closed-CNT/felt is expected to take place in the walls of the cup-stacked or bamboo structures: on the surface and inside the walls. The walls of such structures, mainly in the case of cup-stacked CNTs, are formed by graphene interlayers (see Fig. 1). Lithium insertion into these planes has been detected in bamboo structures [7]. Lithium insertion in open-CNTs could also occur inside the tube channels. The fibers of the felt can also undergo lithium intercalation because their surfaces are not completely closed; i.e., they are permeable to lithium insertion [9].

The cathodic peaks or shoulders observed at potentials above 250 mV for all the voltammograms can be interpreted on the basis of electrolyte decomposition. Peaks associated with cathodic electrolyte decomposition disappear when the solid electrolyte interphase (SEI) is completely formed [15]. In the case of the CNT/felt, the cathodic peak or shoulder at about 1.3 V is due to electrolyte decomposition, and so are the other cathodic peaks at about 0.8 and 0.5 V. This occurs because these peaks tend to disappear with increasing electrode cathodic/anodic charge ratio, thus reflecting SEI formation. The felt also exhibited a structure suitable for lithium insertion, but is quite different from that of CNT and has an SSE of only 1 $m^2\,g^{-1}$, which presents two small shoulders at 0.5 and 0.8 V. Similar peaks have also been observed in the voltammograms of MWCNTs, and they have been correctly associated with electrolyte decomposition [16]. The effect of the electrolyte on the SEI can be verified when we compare Fig. 2b

and d. The use of the PC/DEC/DMC solvent increases the magnitude of the peaks associated with electrolyte decomposition. SEI formation also explains the behavior of the cathodic/anodic charge ratio in the cycles. In general, the larger the specific surface area of the carbon electrode, the larger the imbalance between the cathodic/anodic charges measured during the first discharge/charge cycle. The ratio between the anodic and cathodic charges in the first cycle was calculated for the voltammograms depicted in Fig. 2. This ratio is 63% in Fig. 2a (felt), 61% in Fig. 2b (closed-CNT/felt), 46% in Fig. 2c (open-CNT/felt) in EC/DMC, and 50% in Fig. 2d (closed-CNT/felt) in PC/DEC/DMC. Both the felt electrode (Fig. 2a), which has an SSA of only $1\,m^2\,g^{-1}$, and the CNT/felt with a lower CNT content (Fig. 2b), where each fiber of the felt is partially covered with CNTs and contains nanoparticles of metallic catalyst not used during CNT growth, leading to a smaller imbalance between the charges; in other words, the anodic/cathodic charge ratio in the first cycle is large. For the other composites (Fig. 2c and d), which contain a larger amount of open or closed CNT and thus each fiber of the felt should be completely filled with CNTs, the anodic/cathodic charge ratio decreased. This is probably because the presence of a larger amount of CNTs on the CNT/felt increased the felt SSA. The opening of the tube tips can also contribute to the increased SSA of the composite, since defects in CNTs are good adsorption sites. Summing up, the cathodic/anodic charge ratio for the CNT/felt is influenced by the amount and type of the CNT grown on the felt.

The cathodic peaks at potentials ranging from 0 to 0.5 V, as well as the small shoulder at about 0.25 V (not visible in Fig. 2c), are associated with lithium intercalation. In the anodic scan, it is possible to observe that the CNT/felt voltammograms also contain two peaks at about 0.25, 1.1 V (Fig. 2b and c) and 1.27 V (Fig. 2d). These peaks are always observed for several cycles. Therefore, these peaks are really due to lithium intercalation in the CNT/felt electrode. These two sites could be associated with the fact that we have a mixture of two kinds of carbon nanotubes, the cup-stacked structure and bamboo; that is, there are sites with different potentials for lithium insertion in the cup-stacked and in the bamboo structures.

In an anodic scan above 0.25 V, the CNT/felt electrodes exhibit a capacitive current and an anodic process occurs in the 3.25–4.25 V range. In Fig. 2d, there are other small anodic peaks at 2.07 and 2.84 V as well. In Fig. 2c and d, we also have an anodic and broad peak that can be detected for several cycles. In Fig. 2b, where we have closed-CNT this anodic process increases during the first cycles and is also stabilized thereafter.

We believe that these anodic peaks are probably due to a pseudo-capacitive process involving lithium extraction. Because the profile of the last peak changes with electrolyte and new peaks appear in Fig. 2d, we believe that some kind of adsorption may be affecting these Faradaic process. Anodic electrolyte decomposition is not possible since the anodic current is null in this same potential range in the case of the felt (Fig. 2a).

Our results suggest that the magnitude of these peaks and the voltammograms profiles depend on the loading and on whether the tips of the CNTs on the electrodes are open or closed. Fig. 2a and b show that the loading of CNTs plays a significant role in the electrochemical behavior of the electrode.

The influence of the CNT loading is also clear when we compare the peaks in Fig. 2c and d, which are associated with lithium intercalation at potentials below 1.5 V. Below this value, the solvent should not have any importance in this process. The cathodic peak and the two anodic peaks are more intense for the composite with a larger CNT loading and remains in the same position. On the other hand, the influence of the CNT, whether closed or open can also be seen in these peaks. The peak at about 0 mV in Fig. 2c is more intense than that in Fig. 2d, and the second anodic peak occurs at a lower potential than that in Fig. 2d.

The voltammograms undoubtedly show that this electrode can be used for lithium intercalation and as a capacitor, depending on the applied potential range. Our results show that several changes occur in the electrochemical response of the CNT/felt in lithium electrolytes depending on the loading and type of CNTs (open or closed tips).

Fig. 3 shows the behavior of the felt and the CNT/felt in EC/DMC at a higher scan rate, in the range where the double-layer charge/discharge occurs predominantly. These curves follow the relation $i = AC_d v$, where i is the current, A the area of the electrode, and v is the scan rate. The felt double-layer capacitance (C_d) (Fig. 3a) is much lower than the CNT/felt capacitance (Fig. 3b and c). The magnitude of the current in Fig. 3 again reflects the fact that the CNT loading and type play an important role in the electrochemical properties of the composite, as previously suggested by the voltammograms. For example, the capacitive current taken at 2.6 V for Fig. 3c (open-CNT with 13.93 mg of CNT), for example, is about five times larger than that in Fig. 3b (closed-CNT with 2.11 mg of CNTs), which is much larger than that of the felt alone (Fig. 3a).

Fig. 4 shows the C_d values (taken after several cycles) of the same electrodes used in Fig. 3b and c in EC/DMC, obtained under galvanostatic conditions as a function of the current. The double-layer capacitance was determined so that C_d is equal to the product of the applied current by the polarization time and the voltage variation of during the charge/discharge of the capacitor free of ohmic drop.

The specific C_d curve versus the current of the closed-CNT/felt is taller for the open-carbon nanotubes in spite of the lower mass of CNT in the open-CNT/felt composite. However, if we calculate the capacitance taking the total mass of the composite into account the curve of the closed-CNT/felt is shifted below $9.74\,F\,g^{-1}$, while for the open-CNT/felt the curve is shifted to $4.39\,F\,g^{-1}$. The total capacitance of the open-CNT/felt electrode is thus larger than that of the closed-CNT/felt at all currents applied. This effect shows that felt substrate contributes to the electrode capacitance, besides giving evidence of a small BET area. Voltammetry of the felt (Fig. 2a) showed that it is not a totally inactive substrate for lithium intercalation and/or adsorption. Again, the electrochemical properties of the CNT/felt composite depend predominantly on CNT loading and type. For the closed-CNT/felt composite, the catalyst particle (Mn, Co) could contribute for the capacitance, which also explains the differences between the total and spe-

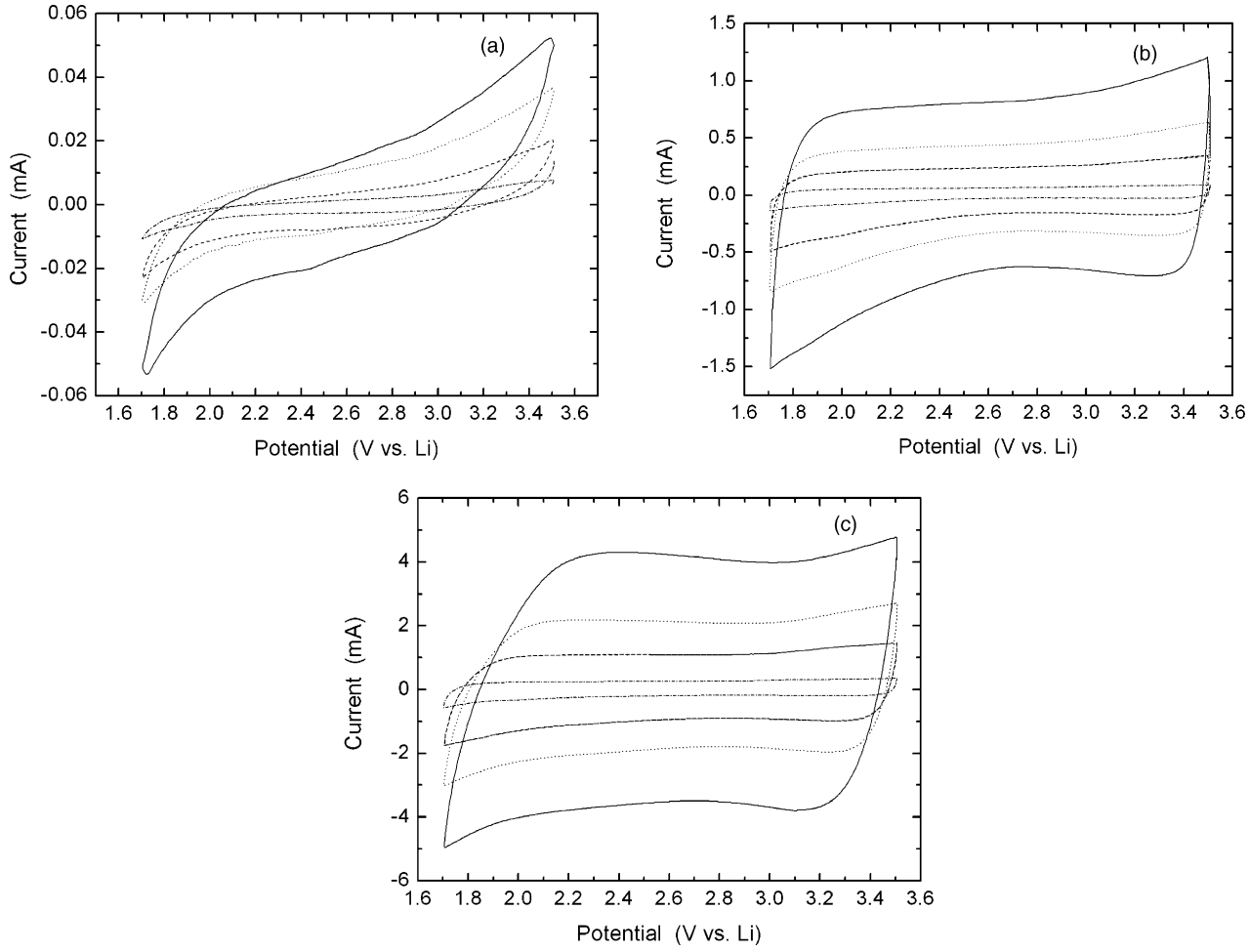

Fig. 3. Voltammograms collected at high scan-rate (20, 10, 5, 1 mV s^{-1}) for the felt (a), the closed-CNT/felt (b), the open-CNT/felt (c). The CNT mass is 2.11 mg in (b) and 13.93 mg in (c).

cific capacity. The mass of catalyst is not used in the specific capacity.

Fig. 4 suggests that the amount of CNT can also have other effects on the CNT/felt composite. Reduction of C_d with increasing current is smaller for the open-CNT/felt than for the closed-CNT/felt. This occurs because the open-CNT/felt composite contains many more CNTs, which should probably imply in a cell with lower electrical resistance. As discussed before, the presence of CNTs is expected to lead to decreased fiber resistance [8]. However, the fact that the cavity and holes of the felt are filled with CNTs should be another important effect on the electrode total resistance. Emission studies in the CNT/felt have shown that the electronic properties of CNT/felt depend on CNT loading [10]. The loading of open-carbon nanotubes is larger than that of closed-carbon nanotubes. We believe that the variations in C_d with current observed in Fig. 4 should thus be associated with the CNT loading.

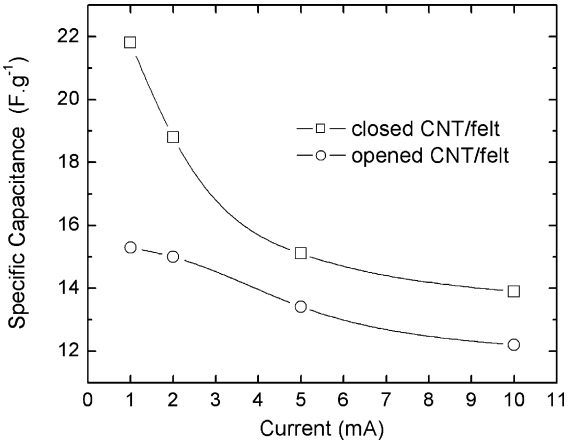

Fig. 4. Specific double-layer capacitance of the open-CNT/felt and closed-CNT/felt used in Fig. 3 as a function of the load current between 1.5 and 3.7 V vs. lithium reference. The capacitance were taken in the 20 cycle for each current.

Because many studies provide the capacity as F cm^2, we have estimated the C_d of the CNT/felt in F cm^2 using the BET area. If we use the SSA obtained for 24.4 mg of open-CNT on the felt, the total C_d of open-CNTs shown in Fig. 4b, which contain lower CNT mass, is about 40.3 μF cm^2 in 10 mA. Calculating the electrochemical area of the CNT/felt is not an easy task. However, if we consider the fact that the composite does not use a binder, and therefore, for all CNTs must be in contact with the electrolyte, the BET area should be a good approximation to carrying out this estimative. In electrodes prepared with a binder

this is a problem because the contact between active material and polymer binder reduces this area.

The C_d obtained for the CNT/felt thus appears to be very interesting from the technological point of view. The C_d values obtained for the CNT/felt composite, as well as the current density (about 4.7–0.47 A g^{-1} for the open-CNT and 0.7–0.07 A g^{-1} for the closed-CNT) support this affirmation. Furthermore, we have carried out studies about the CNT/felt double-layer capacitance in 1 M H_2SO_4, to compare them with other carbon materials. A closed-CNT/felt with CNT loading of 9.3 mg provides about 30 F g^{-1} at 20 mA. Carbon black, active carbon, and graphite clothes in aqueous electrolyte with surface area larger than that of this closed-CNT/felt have lower double-layer capacitance than this closed-CNT/felt [2]. The C_d of the CNT/felt lies in the range of C_d reported for MWCNTs electrodes prepared with polymer binders and submitted to lower current density (i.e. mA g^{-1}) [17–21].

Fig. 5 shows the capacitance behavior of a capacitor assembled with two similar closed-CNT/felt electrodes in EC/DMC under galvanostatic conditions. The voltage range and the applied current were chosen aiming at having charge/discharge of the electric double-layer only (linear variation of potential with time). The potential limits correspond to the potential difference between two electrodes with respect to a lithium potential (reference electrode). The potential of two electrodes were registered during the polarizations and the differences between them were used to discuss the capacitor response. For the capacitor working from 0 to 2.5 and 0 to 3.0 V, the linear regime was possible when a 5 mA constant charge/discharge current was used, due to the anodic electrolyte decomposition and lithium insertion. The open-circuit potential of the CNT/felt is about 3.1 V versus lithium. At $\Delta E \leq 2.0$ V, the best capacitance taken in the 20 cycle is obtained at lower current (11.5 F g^{-1} in 0.09 A g^{-1}), and at $\Delta E = 2$ and 3 V, the capacitance values are also good, (10.6 F g^{-1} in 0.44 A g^{-1}), indicating that the CNT/felt has potential application in the

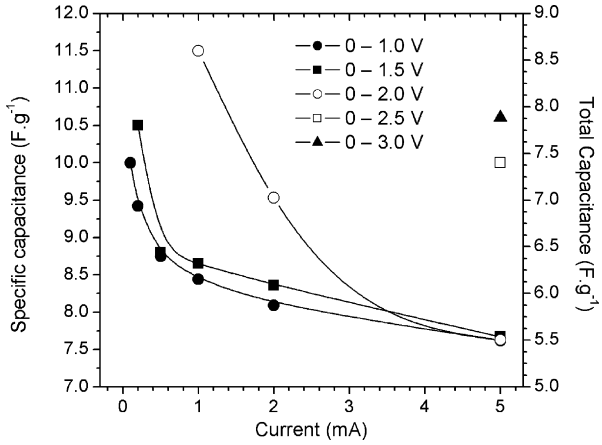

Fig. 5. Specific and total double-layer capacitance of a capacitor prepared with two closed-CNT/felt electrodes as a function of the load current and voltage window. The capacitance were taken in the 20 cycle for each current.

development of capacitors completely free of binders. When we stopped the characterization in the 300 cycle at 1 mA, the capacitance of this capacitor was identical to shown in Fig. 5.

The behavior of the CNT/felt for energy storage was analyzed on the basis of lithium intercalation. Fig. 6A shows the first discharge/charge of the open-CNT/felt and its specific capacity for charge/discharge cycles using 5 mA as the load current in EC/DMC. After the 10th cycle, the reversible specific capacity was found to remain stable over 50 cycles when the electrode current was changed to a lower value (Fig. 6B).

During the first cycle (Fig. 6A), the irreversible specific capacity associated with SEI formation was 153 mAh g^{-1}. After the first cycle, the specific capacity for cathodic and anodic polarization became similar and then stabilized at about 125 mAh g^{-1} in successive cycles. It is worth noting that, in Fig. 6A, the composite seems to have an additional capacity in anodic polarization between 1.5 and 4.0 V versus lithium. This confirms

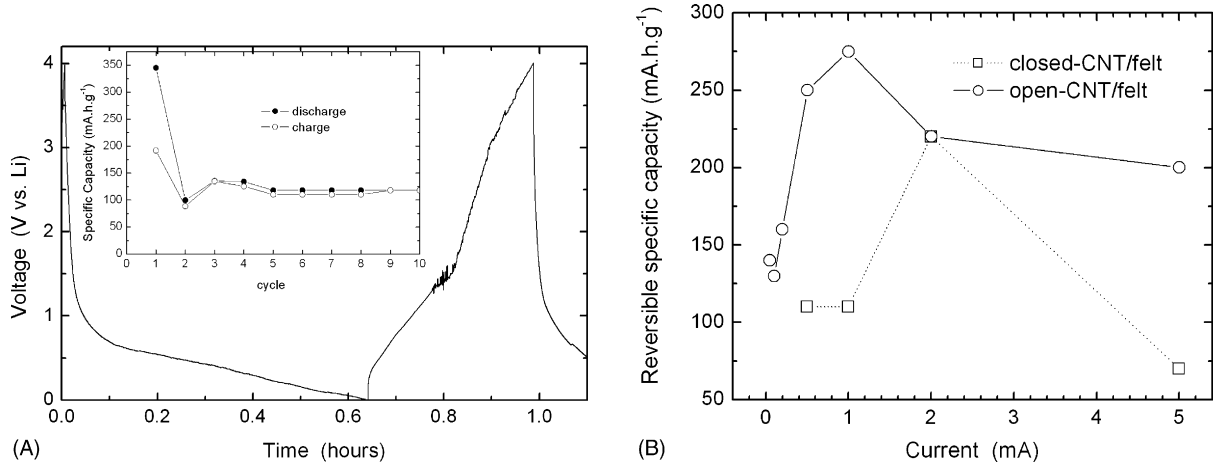

Fig. 6. First discharge/charge of the open-CNT/felt electrode at 5 mA and its specific capacity (inner picture) as a function of the number of discharge/charge cycles (A) and the variation in the reversible total capacity taken in the tenth cycle as a function of the load current (B). All capacities were obtained between 4 V and 0.001 mV vs. lithium potential. In the highest discharge/charge rate, the gravimetric current for the composite open-CNT/felt is 0.4 A g^{-1} (total mass of the electrode) and 0.8 A g^{-1} (CNT mass), while for the closed-CNT/felt these values are 0.30 and 0.78 A g^{-1}, respectively.

that the additional peaks observed in the voltammograms in this range are due to a Faradaic process.

The capacity behavior as a function of the current applied to the composite is shown in Fig. 6B. This curve was obtained for closed-CNT/felt and open-CNT/felt with similar CNT loadings. The electrodes were initially polarized in 5 mA and the capacity was taken in the in the tenth cycle. Then, the current was decreased. The irreversible capacity was observed in the first cycles only. For the closed-carbon nanotubes, it was found to be 100 mAh g^{-1}, instead of 125 mAh g^{-1} observed for the open-carbon nanotubes.

There is an anomalous effect in the reversible capacity associated with decreasing current in the case of both electrodes (Fig. 6B). The reversible specific capacity increases with decreasing current until a maximum is reach, and it decreases thereafter. An anomalous behavior was also found in closed MWCNT, where the reversible capacity increased with increasing current too [22]. This anomalous effect was associated with the presence of two different for intercalation sites, which suggests that in our case there also are different sites for lithium intercalation, with different kinetics, thus providing different specific reversible capacities depending on the current applied to the electrode. In fact, the maximum specific reversible capacity occurs at different current values. For the open-CNT/felt, the maximum reversible specific capacity occurs at 1 mA, while for closed-CNT/felt it is found at 2 mA. Thus, a better understanding of the mechanism of lithium insertion into the cup-stacked and bamboo-like CNT structures is required. The effect of open tubes in this structure should be investigated.

Finally, it is interesting to analyze the values of specific capacity observed for the CNT/felt composite. In the case of the open-CNT/felt, the reversible specific capacity is able to provide 275 mAh g^{-1} at 0.16 A g^{-1} and 200 mAh g^{-1} at 0.82 A g^{-1}, but only 125 mAh g^{-1} at 16.4 mA g^{-1}. The reversible specific capacities of MWCNT or SWCNTs reported in the literature as 16.4 mA g^{-1} at low current are superior to this value. The way MWCNT and SWNTs tubes are agglomerated in the electrode affects their capacities, because several sites or micropores might be created when the tubes are randomly stacked [23]. These additional sites for the lithium storage may explain why the capacities observed for carbon nanotube electrodes depend on the preparation method. In the case of the CNT/felt, the N_2 isotherms show the absence of pores, which is reasonable considering the fact that each tube grows vertically on the surface of the felt fiber. The irreversible capacity of the CNT/felt in the first cycle is similar to the best values obtained in literature for other CNTs [21,24]. The irreversible capacity of the lithium ion battery can be overcome with a mass balance between the electrodes. Besides the anomalous effect of the CNT/felt prepared herein and its low reversible specific capacity at low current, its capacity at higher gravimetric density is attractive for lithium ion battery. If we consider the dimension of the CNT/felt electrodes studied in this work (disc with a diameter of 7 mm), they seem to be competitive with respect to the carbon electrodes prepared with binders at higher gravimetric current densities.

4. Conclusions and summary

In this paper we showed the electrochemical performance of CNT/felt electrodes as capacitors and electrodes for lithium intercalation for the first time. The CNTs were grown on a conductive carbon felt by the CVD method, which means that it is possible to obtain electrodes whose area, shape, and thickness are limited essentially by the dimensions of the furnace used during the synthesis. The three-dimensional structure of the felt allows incorporation of higher amounts of CNT than those obtained in the case of other carbon substrates like vitreous carbon and carbon tissue used in energy devices.

High resolution transmission electronic microscopy showed that, in the case of CNT/felt composite prepared from methanol decomposition, the CNTs are of the cup-stacked and bamboo-like types.

The double-layer capacitance values and the specific capacity at high gravimetric current density show that the CNT/felt opens interesting perspectives for the development of flat, cylindrical devices free of polymer binder. The electrochemical performance of the composite was found to depend on all the components present in the composite: CNT (type and loading), felt, catalyst not used in the CNT growth. This means that many improvements in the electrochemical performance obtained by this new approach could be applied since it is an electrode completely free of binder. The influence of the catalyst can be observed when the total composite mass used in the studies shows that the incorporation of nanoparticles is the natural step toward the improvement in the capacitance and specific capacity of the CNT/felt. Changes in felt conductivity are also another way to improve the performance of the composite.

We believe that the interesting performance of the CNT/felt both as a capacitor and battery electrode at higher gravimetric current density is associated with its low electrical resistance, since we only have carbon materials with high electronic conductivity. The CNTs were grown on a carbon fiber, which means that the electrical resistance between the fiber and carbon nanotubes should be lower than on carbon nanotubes and polymer binder, carbon nanotubes, and other non-carbon substrates.

The CNT/felt also exhibits mechanical stability with respect to cutting and to chemical treatments such reflux at high temperature. We see that the electrode can be submitted to several cycles, while remaining intact. This is reasonable since the CNT is connected to the carbon substrate via a chemical bond, and not by a polymer as in the case of binder-containing electrodes. In the latter cases, the electrode mechanical stress provoked by lithium intercalation can result in electrode degradation, thus leading to a fading capacity.

The possibility of exposing the total mass of the CNT mounted on the electrode is another factor that explains its electrochemical performance at higher gravimetric current densities. The CNT/felt is a three-dimensional web of CNTs, and the carbon fiber allows a percolation that cannot be easily obtained in electrodes prepared with a binder.

The thermal stability of the CNT/felt is limited to the carbon stability, which means that it can be used at temperatures higher

than those employed in the case of polymer binders. This means that this composite electrode could be very useful for electrochemical devices of interest for electric vehicles [25–27]. An electrochemical study involving composites based on the growth of single-walled carbon nanotubes and multi-walled carbon nanotubes and oxide nanoparticles on felt are underway in our group and will be published elsewhere.

Acknowledgements

This work is supported by FAPESP (04/07085-2), CNPq. The authors would like to thank LME/LNLS for technical support during the electron microscopy work.

References

[1] G. Pistoia, Lithium Batteries, 1st ed., Elsevier, New York, 1994, pp. 1–483.
[2] B.E. Conway, Electrochemical Supercapacitors, 1st ed., Kluwer Academic, New York, 1999, pp. 1–698.
[3] M.S. Dresselhaus, G. Dresselhaus, P.C. Eklund, Science of Fullerenes and Carbon Nanotubes, 1st ed., Academic Press, New York, 1996, pp. 1–965.
[4] T.W. Ebbesen, Carbon Nanotubes, 1st ed., CRC Press, New York, 1997, pp. 1–304.
[5] I.R. de Moraes, W.J. da Silva, S. Tronto, J.M. Rosolen, J. Power Sources, in press.
[6] C. Kim, Y.J. Kim, Y.A. Kim, T. Yanagisawa, K.Ch. Park, M. Endo, M.S. Dresselhaus, J. Appl. Phys. 96 (2004) 5903–5905.
[7] D.Y. Zhong, G.Y. Zhang, S. Liu, E.G. Wang, Q. Wang, H. Li, X.J. Huang, Appl. Phys. Lett. 75 (1999) 3105.
[8] J.M. Rosolen, S. Tronto, M.S. Marchesin, E.C. Almeida, N.G. Ferreira, C.H.P. Poá, S.R.P. Silva, Appl. Phys. Lett. 88 (8) (2006), 083116–083116(3).
[9] E.C. Almeida, N.G. Ferreira, J.M. Rosolen, Diamond Relat. Mater. 14 (2005) 1673–1677.
[10] J.M. Rosolen, C.H.P. Poá, S. Tronto, M.S. Marchesin, S. Ravi, P. Silva, Chem. Phys. Lett. 424 (2006) 151–155.
[11] E. Frackowiak, F. Béguin, Carbon 40 (2002) 1775–1787.
[12] Z.H. Yang, H.Q. Wu, Solid State Ionics 143 (2001) 173–180.
[13] G. Maurin, Ch. Bousquet, F. Henn, P. Bernier, R. Almairac, B. Simon, Chem. Phys. Lett. 312 (1999) 14–18.
[14] A. Udomvech, T. Kerdcharoen, T. Osotchan, Chem. Phys. Lett. 406 (2005) 161–166.
[15] G.E. Blomgren, J. Power Sources 81/82 (1999) 112–118.
[16] H.-C. Shin, M. Liu, B. Sadanadan, A.M. Rao, J. Power Sources 112 (2002) 216–221.
[17] M. Endo, Y.J. Kim, T. Chino, O. Shinya, Y. Matsuzawa, H. Suezaki, et al., Appl. Phys. A 82 (2006) 559–565.
[18] Y.T. Kim, T. Mitani, J. Power Sources, in press.
[19] S. Shiraishi, M. Kbe, T. Yokoyama, H. Kurihara, N. Patel, A. Oya, et al., Appl. Phys. A 82 (2006) 585–591.
[20] Z. Yang, Y. Feng, Z. Li, S. Sang, Y. Zhou, L. Zeng, J. Electroanal. Chem. 580 (2005) 340–347.
[21] J.Y. Eorn, D.Y. Kim, H. Kwon, J. Power Sources, in press.
[22] Q. Wang, L. Ku, L. Chen, X. Huang, J. Electrochem. Soc. 151 (2004) A1333–A1337.
[23] L.A. Montoro, J.M. Rosolen, Carbon, in press.
[24] E. Frackowiak, S. Gautier, H. Gaucher, S. Bonnamy, F. Beguin, Carbon 37 (1999) 61–69.
[25] P. Thounthong, S. Raël, B. Davat, J. Power Sources 153 (1) (2006) 145–150.
[26] C. Ashtiani, R. Wright, G. Hunt, J. Power Sources 154 (2) (2006) 561–566.
[27] D. Aurbach, J. Power Sources 146 (1/2) (2005) 71–78.